

Characterizing the Hexagonality of Anodic Aluminium Oxide Nanoporous Arrays

Luciano da Fontoura Costa*

*Instituto de Física de São Carlos, Universidade de São Paulo,
Av. Trabalhador São Carlense 400, Caixa Postal 369,
CEP 13560-970, São Carlos, São Paulo, Brazil*

Gonzalo Riveros

*Departamento de Química, Facultad de Ciencias,
Universidad de Chile, P.O. Box 653, Santiago de Chile, Chile.*

Humberto Gómez, Andrea Cortes

*Instituto de Química, Facultad de Ciencias,
Universidad Católica de Valparaíso, Casilla 4059, Valparaíso, Chile.*

Maxime Gilles, Enrique A. Dalchiele, Ricardo E. Marotti

*Instituto de Física, Facultad de Ingeniería,
Julio Herrera y Reissig 565, C.C. 30, 11000, Montevideo, Uruguay.*

(Dated: 15th March 2005)

Abstract

Nanoporous anodized alumina oxide have been used as templates for obtaining nanomaterials such as nanowires, which exhibit interesting electronic, magnetic and optical properties. This article presents how the regularity of the spatial distribution of pores in such templates, which affects several of the physical properties of the obtained nanomaterials, has been objectively quantified. The method uses adaptive thresholding, wave propagation image analysis methods, as well as an hexagonality measurement which was found to be particularly suitable because of its locality and invariance to translation, rotation and scaling. A comparison between commercial and laboratory-made samples is presented in order to test the method, resulting higher hexagonality for the latter type of templates.

*Electronic address: luciano@if.sc.usp.br

I. INTRODUCTION

Nanoporous alumina (Al_2O_3) obtained by anodizing aluminum has emerged as an interesting template for nanomaterials [1], [2]. The resulting porous anodic aluminum oxide (AAO) has pore diameter that can be varied from approx. 10 nm for the smallest pores, to approx. 300 nm for the largest pores, depending on the details of the anodizing electrochemical process (mainly electrolyte and potential). The depth of the pore depends basically on the duration of the process, which allows almost perfectly aligned cylindrical pores with a depth as large as approx. 100 μm [3]. With this high aspect ratios it is possible to grow both metallic and semiconductor nanowires [4], [5], [6] or nanotubes [7] inside the pores. These nanostructures can have interesting electronic transport properties [7], [8], [9] and magnetic properties, significantly different from the same bulk material [10], [11]. In any case, the optical properties of the AAO templates alone have shown interesting anisotropic [12] and luminescent properties, not yet well understood [13], [14]. Altogether with the simple and inexpensive preparation process, AAO appears as an interesting nanostructured material template with potential for applications in electronic, photonic and magnetic nanodevices. Moreover, under certain deposition conditions, the nanopores distribution in the final material is highly ordered [1], [2], [15], with an almost hexagonal distribution. This particular geometry is suitable for many applications in both quantum electronic effects and photonic crystals. Indeed, although the properties of the metallo-dielectric composite has been studied long ago [16], their implication for 2D photonic crystals has been recently placed into evidence [17], [18], [19].

For all the previous many applications of nanoporous AAO the characterization of both size and distribution of the resulting material is very important. The usual characterization method of the hexagonal ordering is made by taking the Fast Fourier Transformation (FFT) of a 2D image of the surface of the AAO samples [15], [20], [21]. However, this method requires a high orientational order in the whole region under study, and consequently cannot take appropriate account of the short range hexagonal ordering of the AAO samples. The current work describes how physics-based image analysis methods have been applied in order to obtain the proper identification of the pores centers and to quantify the spatial regularity of such spatial structure in terms of an hexagonality measurement. This feature is particularly suitable because of its locality and invariance to translations, rotations, and

scaling. The application of such a methodology has indicated that alumina arrays specifically prepared for this work (from now on referred to as *laboratory-made*) present substantially higher hexagonality than commonly used commercial arrays [6, 17].

II. MATERIALS AND METHODS

A. Sample Preparation and Characterization

For the present study the AAO arrays have been fabricated by the following process according to the two step electrochemical anodization [1], [22]. First, high purity (99.95%) aluminum foils were degreased in hot acetone and after that ultrasonically cleaned in isopropyl alcohol. Then, the samples were annealed at 350 °C for 1 hour in air. Subsequently, they were submitted to a chemical etching in dilute nitric acid and then in 5% NaOH at 60 °C for 30 s. Afterwards, the aluminum was first mechanically polished and then electropolished in a 2:2:4 weight mixture of $H_2SO_4:H_3PO_4:H_2O$. Then, the aluminum samples was submitted to a first anodization process at 40 V_{DC} in a 0.3 M oxalic acid solution at either 2 °C or 20 °C, until an alumina layer thickness of ca. 8 μm was achieved. The electrolyte was rigorously stirred during anodization. After that, and only for some samples, this AAO was dissolved away by immersing the specimens in a mixed solution of 6%(wt) H_3PO_4 and 1.8%(wt) CrO_3 at 60 °C for 1 hour. Subsequently, the aluminum sheets were anodized in the same conditions described above for 6 hours. Consequently, an AAO array with highly ordered pore arrays were obtained. The specific treatment to which each sample was submitted is described in Table I.

For comparison, commercial ANOPORE/registered alumina membranes purchased from the Whatman Company, with 20nm nominal pore size, were used. The AAO arrays were imaged by using a scanning electron microscopy (SEM) JEOL 5900 LV SEM equipment.

B. Image Analysis Concepts and Methods

The obtained gray-level images presented intensity fluctuations and noise which complicated the automated identification of the pores. In order to cope with this problem, an adaptive thresholding method [24] was applied which involved the calculation, for each pixel $p(x, y)$, of the average gray level $\langle p_R(x, y) \rangle$ along a circular window with radius of R pixels.

Sample	id.	TT	EP	t ₁	T ₁ (°C)	t ₂	T ₂ (°C)	av.hexag.± st.dev
commercial membrane	1	-	-	-	-	-	-	0.413 ± 0.085
	2	-	-	-	-	-	-	0.375 ± 0.073
	3	-	-	-	-	-	-	0.400 ± 0.077
	4	-	-	-	-	-	-	0.393 ± 0.077
laboratory made	5	No	Yes	6 hrs.	2±1	-	-	0.521 ± 0.123
	6	Yes	No	6 hrs.	2±1	-	-	0.533 ± 0.121
	7	Yes	Yes	6 hrs.	2±1	-	-	0.472 ± 0.112
	8	Yes	No	2 hrs.	2±1	6 hrs.	2±1	0.532 ± 0.116
	9	Yes	YEs	25 min	20±1	6 hrs.	20±1	0.545 ± 0.119

After subtracting such a value from $p(x, y)$, the result is compared with a threshold T . In case $\langle p_{10}(x, y) \rangle - p(x, y)$ is smaller than T , the pixel at (x, y) is understood to belong to the core of the pore. The values of the involved parameters may vary from image to image. All cases treated in the current work assumed $R = 10$ and varying thresholds.

The adaptive thresholding described above produces clusters of pixels at the core of those pores which have a minimal contrast quality, so that pores which are faded or which present low contrast are disregarded. Because the clusters of points obtained at the center of each identified pore may appear disconnected, the closing operation from mathematical morphology [24] is applied in order to ensure that a single connected cluster is obtained at the center of each pore.

Once the connected groups were properly obtained, they were labeled with consecutive integer values, ranging from 1 to N_p , where N_p is the number of pores identified in each image. The center of mass of each connected group was obtained and used to represent the center of each pore, which is henceforth called a *seed*. Constant speed propagating wavefronts [23, 24, 25] were then initiated simultaneously at each of such centers, which was performed by using the distance-based dilations described in [24, 25], so that the shocks between waves emanating from different seeds corresponded to the boundaries of the respective Voronoi tessellation. Such a tessellation has the interesting property that every point inside each cell

is closer to the respective seed than to any other seed.

For each Voronoi cell, the adjacent cells were obtained by searching for neighboring pixels with different labels while following the cell boundary in clockwise fashion. Such an approach allowed the adjacent seeds, namely those having a boundary with the reference cell, to be obtained in suitable order for calculation of the angles. Figure 1(a) shows a reference seed i (black dot) and four of its adjacent seeds (white dots). The successive angles are represented as $\alpha_1, \alpha_2, \dots, \alpha_{N_i}$, where N_i is the number of neighbors of the reference seed i . The hexagonality index h_i of each cell i can now be defined as in Equation 1. Those cells which are adjacent with the image borders are excluded from calculation.

$$h_i = \left(\sum_{k=1}^{N_i} |\alpha_k - \pi/3| + 1 \right)^{-1} \quad (1)$$

This measurement can be verified to vary from 0 to 1. Because this index only takes into account the angles between the reference seed and those seeds which are adjacent to it, when applied to a single cell it may produce maximum value of 1 for cells defined by adjacent cells which are at different distances from the reference seed. However, when applied to all cells of a nanoporous arrays, higher average hexagonality values are obtained only for a nearly hexagonal structure, assuming smaller values otherwise. Indeed, hexagonality densities characterized by all values equal to 1 can only be obtained for perfectly hexagonal structures. This is because the presence of cells with correct angles but varying distances from adjacent seeds will necessarily imply perturbations to the neighboring cells, disrupting the respective angles and reducing the hexagonality indices.

The hexagonality index is invariant to the position, rotation and size of the image or portions of it. Moreover, the index value depends only on the immediate neighborhood of the reference seed and therefore is not affected by other parts of the image, as would be the case with global methods such as those based on the Fourier transform. This feature allows the proper quantification of the structural uniformity even in the case where the arrays contain several domains of hexagonal structures with different preferential orientations.

III. RESULTS AND DISCUSSION

Figure 2 illustrates the application of the adopted structural analysis. The original images of a commercial membrane (a) and a laboratory-made alumina template (e) samples were processed in order to obtain the gray-level uniformization and seeds, shown in (b) and (f). The Voronoi tessellations obtained from the previous seeds are shown in (c) and (g). Note that the different gray-levels correspond to the distinct labels assigned to each Voronoi cell. The hexagonality densities of the commercial membranes and laboratory-made templates are given in (d) and (h), respectively. It is clear from such densities that the laboratory-made samples yielded substantially higher hexagonality values, corroborating the higher spatial organization indicated by visual inspection of figures (a) and (e).

The average \pm standard deviations of the hexagonalities obtained for a set of 4 commercial membranes and 5 laboratory-made alumina samples are given in the last column of Table I, further corroborating the higher structural uniformity of the laboratory-made nanoporous templates. In effect, it is clearly seen that for all except one of the laboratory-made samples the mean value of the hexagonality defined by equation (1) is greater than 0.5, while it remains below this number for the commercial membrane. Moreover the highest values are obtained for the two samples submitted to both anodization process (samples 8 and 9). Althought the values are similar for samples 5 and 6 (and quite smaller for sample 7), their deviation is slightly smaller for samples 8 and 9. This corroborates the contribution of the second anodization process in increasing the nanoporous ordering [20, 21].

Note that the standard deviation values of the hexagonalities shown in Table I for the laboratory-made samples are in all cases greater than the values obtained for the commercial membranes. These results must be compared with the hexagonalities distributions shown in Figure 2 (d) and (h). For the commercial membrane, Figure 2 (d), the distribution is almost symmetric, while for the highly-ordered laboratory-made samples, Figure 2 (h), the distribution is quite assymmetric. This assymmetry, that may be originated in the self organization process which leads to the ordering of the nanopore array, has its maximum in a value greater than its mean value, implying the increase of the standard deviation for the laboratory-made samples.

IV. CONCLUDING REMARKS

We have shown how the structural uniformity of nanoporous template, which have several interesting properties and applications, can be quantified by using powerful image and shape analysis concepts and methods, including image correction, mathematical morphology and Voronoi diagrams. By taking into account the angular regularity of individual Voronoi cells, the hexagonality index resulted local and invariant to position, rotation and scaling of the cells, allowing the proper quantification of the overall hexagonality even in cases where the arrays exhibit several domains with different preferential orientations. By using such a methodology, it was possible to conclude that the laboratory-made AAO samples present higher structural uniformity than commercial membranes, and samples with second anodization process have higher regularity. Future works include the application of similar analysis to very highly ordered structures, as well as the extension of the present image treatments for the determination of other parameters such as pore diameter and interpore-distance.

Acknowledgments

LDFC thanks FAPESP (proc. 99/12765-2) and CNPq (proc. 3082231/03-1) for financial support. G.R., H.G. and A.C. thank FONDECYT (Chile). E.A.D. and R.E.M. thank to CSIC (Universidad de la Republica) and to PEDECIBA-FISICA, Uruguay. The authors are also grateful to J. Troccoli and A. Marquez for SEM measurements.

- [1] H. Masuda, K. Fukuda, *Science*, **268**, 1466 (1995).
- [2] O. Jessensky, F. Mller, U. Gosele, *Appl. Phys. Lett.* **72**, 1173 (1998).
- [3] S. A. Knaack, M. Redden, M. Onellion, *Am. J. Phys.* **72**, 856 (2004).
- [4] Z. Zhang, D. Gekhtman, M. S. Dreselhaus, J. Y. Ying, *Chem. Mater.* **11**, 1659 (1999).
- [5] Y. C. Wang, I. C. Leu, M. H. Hon, *J. Appl. Phys.* **95**, 1444 (2004).

[6] G. Riveros, H. Gomez, A. Cortes, R. E. Marotti, E. A. Dalchiele, *Appl. Phys. A*, Ref# DOI: 10.1007/s00339-004-3112-1.

[7] W. Young Jang, N. N. Kulkarni, C. K. Hih. Z. Yao, *Appl. Phys. Lett.* **84**, 1177 (2004).

[8] Z. Zhang, X. Sun, M. S. Dreselhaus, J. Y. Ying, J. Heremans, *Phys. Rev. B* **61**, 4850 (2000).

[9] F. Elhoussine, S. Matefi-Tempfli, A. Encinas, L. Piraux, *Appl. Phys. Lett.* **81**, 1681 (2002).

[10] M. Zheng, L. Menon, H. Zeng, Y. Liu, S. Bandyopadhyay, R. D. Kirby, D. J. Sellmyer, *Phys. Rev. B*, **62**, 12282 (2000).

[11] Y.-G. Guo, L.-J. Wan, C.-F. Zhu, D.-L. Yang, D.-M. Chen, C-L. Bai, *Chem. Mater.* **15**, 664 (2003).

[12] A. C. Galca, E. S. Kooij, H. Wormeester, C. Salm, V. Leca, J. H. Rector, B. Poelsema, *J. Appl. Phys.* **94**, 4296 (2003).

[13] G. S. Huang, X. L. Wu, Y. F. Mei, X. F. Shao, G. G. Siu, *J. Appl. Phys.* **93**, 582 (2003).

[14] W. L. Xu, M. J. Zheng, S. Wu, W. Z. Shen, *Appl. Phys. Lett.* **85**, 4364 (2004).

[15] L. Ba, W. S. Li, *J. Phys. D: Appl. Phys.* **33**, 2527 (2000).

[16] D. G. W. Goad, M. Moskovits, *J. Appl. Phys.* **49**, 2929 (1978).

[17] N. Garcia, E. V. Ponizowskaya, H. Zhu, J. Q. Xiao, A. Pons, *Appl. Phys. Lett.* **82**, 3147 (2003).

[18] N. Garcia, E. V. Ponizowskaya, J. Q. Xiao, , *Appl. Phys. Lett.*, **80**, 1120 (2002)

[19] J. B. Pendry, A. J. Holden, W. J. Stewart, I. Youngs, *Phys. Rev. Lett.*, **76**, 4773 (1996).

[20] S. Shingubara, K. Morimoto, H. Sakaue, T. Takahagi, *Electrochem. Solid-State Lett.* **7**, E15 (2004).

[21] G. D. Sulka, S. Stroobants, V. Moshkalkov, G. Borghs, J. P. Cells, *J. Electrochem. Soc.* **149**, D97 (2002).

[22] H. Masuda, K. Yada, A. Osaka, *Jpn. J. Appl. Phys.* **37**, L 1340 (1998).

[23] J. A. Sethian, *Level Set Methods and Fast Marching Methods*, Cambridge Univ. Press (1999).

[24] L. da F. Costa, R. M. Cesar Jr., *Shape Analysis and Classification*, CRC Press (2001).

[25] L. da F. Costa, G. Mutinari, D. Schubert, *Phys. Rev E* **68**, 056704 (2003), cond-mat/0305010.

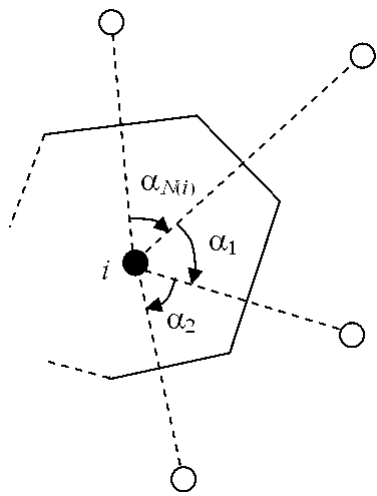
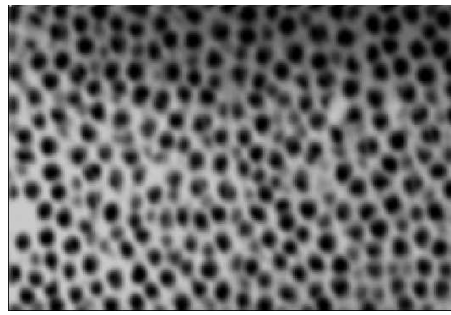
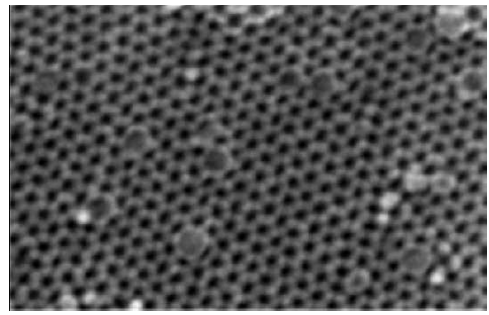


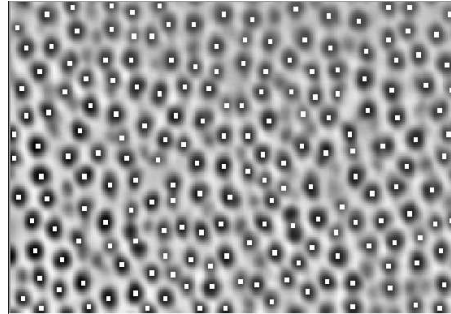
FIG. 1: Figure 1.



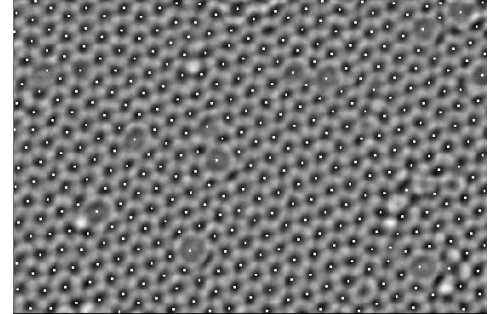
(a)



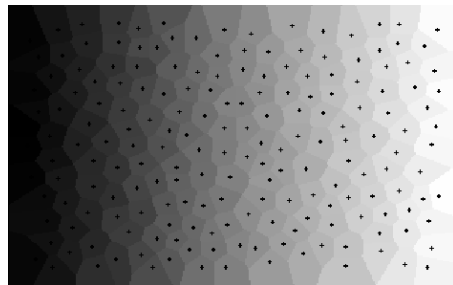
(e)



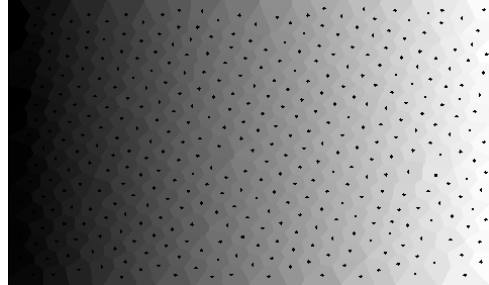
(b)



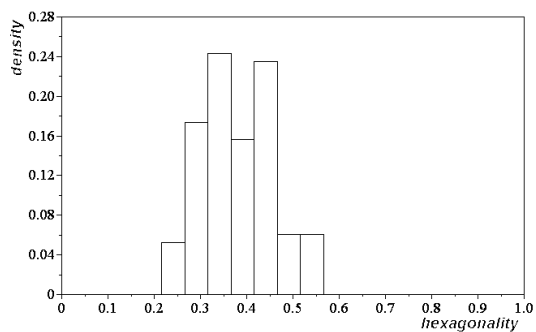
(f)



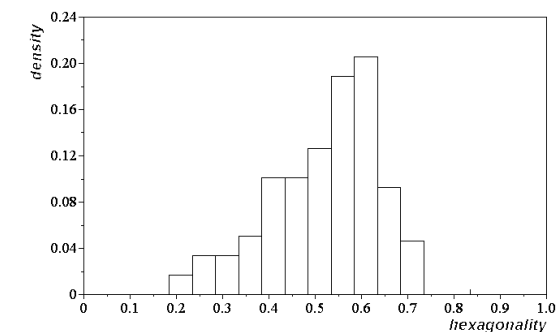
(c)



(g)



(d)



(h)

FIG. 2: Figure 2.

LIST OF CAPTIONS:

Figure 1: Generic Voronoi cell and adopted symbols.

Figure 2: Samples of original commercial (a) and laboratory-made alumina template (e); respective seeds superimposed onto the uniformized images (b) and (f); respective Voronoi tessellations (c) and (g) and densities of the obtained hexagonalities (d) and (h). It is clear from the laboratory-made alumina template exhibits substantially higher hexagonality than the commercial counterpart.

Table I: Description of each sample preparation steps and respective hexagonalities. TT stands for thermal treatment (annealing), and EP for electropolishing. T and t corresponds to temperature and time respectively to the first anodization (subscript 1) and second anodization (subscript 2). Samples 5, 6 and 7 were submitted to just one anodization process. The hexagonalities are given in terms of their averages \pm standard deviations.